

A low CMB variance in the WMAP data

C. Monteserín^{1,2}, R.B. Barreiro¹, P. Vielva¹, E. Martínez-González¹,
M.P. Hobson³ and A.N. Lasenby³

¹ *Instituto de Física de Cantabria, CSIC-Univ. de Cantabria, Avda. de los Castros s/n, 39005 Santander, Spain*

² *Dpto. de Física Moderna, Univ. de Cantabria, Avda. de los Castros s/n, 39005 Santander, Spain*

³ *Astrophysics Group, Cavendish Laboratory, J.J. Thomson Avenue, Cambridge CB3 0EH*

2 August 2021

ABSTRACT

We have estimated the CMB variance from the three-year WMAP data, finding a value which is significantly lower than the one expected from Gaussian simulations using the WMAP best-fit cosmological model, at a significance level of 98.7 per cent. This result is even more prominent if we consider only the north ecliptic hemisphere (99.8 per cent). Different analyses have been performed in order to identify a possible origin for this anomaly. In particular we have studied the behaviour of single radiometers and single year data as well as the effect of residual foregrounds and $1/f$ noise, finding that none of these possibilities can explain the low value of the variance. We have also tested the effect of varying the cosmological parameters, finding that the estimated CMB variance tends to favour higher values of n_s than the one of the WMAP best-fit model. In addition, we have also tested the consistency between the estimated CMB variance and the actual measured CMB power spectrum of the WMAP data, finding a strong discrepancy. A possible interpretation of this result could be a deviation from Gaussianity and/or isotropy of the CMB.

Key words: cosmic microwave background - methods: data analysis - methods: statistical

1 INTRODUCTION

The study of the anisotropies of the cosmic microwave background (CMB) constitutes one of the most powerful tools of cosmology, providing us with very valuable information about the origin and evolution of the universe. In particular, the determination of the CMB power spectrum allows one to put tight constraints on the cosmological parameters. In addition, the study of the CMB temperature distribution provides us with a powerful test of the standard inflationary theory, since this predicts that the CMB fluctuations should follow a homogeneous and isotropic Gaussian distribution whereas alternative theories – such as non-standard inflation (Bartolo et al. 2004) or topological defects (Durrer 1999) – give rise to non-Gaussian fluctuations.

Given the interest of the subject, a large number of techniques have been proposed for studying the Gaussianity and isotropy of the CMB including, among others, the Minkowski functionals (Coles 1988; Gott et al. 1990), the bispectrum (Ferreira, Magueijo & Górski 1998; Heavens 1998; Magueijo 2000), properties of hot and cold spots (Coles & Barrow 1987; Martínez-González et al. 2000), geometrical es-

timators (Barreiro, Martínez-González & Sanz 2001; Doré, Colombi & Bouchet 2003; Monteserín et al. 2005, 2006), extrema correlation function (Naselsky & Novikov 1995; Barreiro et al. 1998; Heavens & Sheth 1999), wavelet analysis (Hobson, Jones & Lasenby 1999; Barreiro et al. 2000; Barreiro & Hobson 2001; Aghanim, Forni & Bouchet 2001), bipolar power spectrum (Hajian & Souradeep 2003), phase analysis (Chiang, Naselsky & Coles 2004) and goodness of fit tests (Aliaga et al. 2005; Rubiño-Martín et al. 2006; Curto et al. 2007).

Many non-Gaussianity analyses have been performed using the best CMB data available up to date, which have been provided by the NASA Wilkinson Microwave Anisotropy Probe (WMAP) satellite (Bennett et al. 2003a, Spergel et al. 2007). The WMAP team carried out a study of the CMB temperature distribution of the first year data (Komatsu et al. 2003) finding that the data were consistent with Gaussianity. However, in subsequent works, a number of unexpected results regarding the Gaussianity and/or isotropy of the CMB were reported, including anomalies related to low multipoles (de Oliveira-Costa et al. 2004; Copi et al. 2004; Land & Magueijo 2005a; Schwarz et al.

2004), north/south asymmetries (Eriksen et al. 2004; Hansen, Banday & Górski 2004a; Hansen et al. 2004b; Eriksen et al. 2005; Land & Magueijo 2005b; Bernui et al. 2006), a cold spot in the southern hemisphere (Vielva et al. 2004; Mukherjee & Wang 2004; Cruz et al. 2005, 2006; McEwen et al. 2005; Cayón et al. 2005), structure alignment (Wiaux et al. 2006), phase correlations (Chiang, Naselsky & Verkhodanov 2003; Coles et al. 2004) and to the amplitude of hot and cold spots (Larson & Wandelt 2004).

After the release of the three-year WMAP data in March 2006, similar analyses have been carried out confirming the presence of the anomalies in the data (Martínez-González et al. 2006; McEwen et al. 2006; Vielva et al. 2007; Cruz et al. 2007; Copi et al. 2007; Bernui et al. 2007; Eriksen et al. 2007; Wiaux et al. 2008).

In this work, we report a new anomaly in the WMAP data: a significantly low value of the CMB variance with respect to the one expected for the WMAP best-fit model. The outline of the paper is as follows. In §2 several quantities related to the one-point density function (1-pdf) are studied for the WMAP data, including the dispersion, skewness, kurtosis and Kolmogorov-Smirnov distance. In §3 the CMB dispersion from the WMAP data is estimated, finding that its value is significantly low. The effect on our results of possible residual foregrounds or systematics are studied in §4. In §5 possible explanations for the anomaly are discussed, including the modification of the cosmological parameters and a deviation of the CMB from Gaussianity and/or isotropy. Finally, our conclusions are presented in §6.

2 TESTS OF GAUSSIANITY BASED ON THE 1-PDF

The NASA WMAP satellite was launched in the summer of 2001. The first-year and three-years results were presented in February 2003 and March 2006 respectively. WMAP observes at five frequency bands: K (22.8 GHz, one receiver), Ka (33.0 GHz, one receiver), Q (40.7 GHz, two receivers), V (60.8 GHz, two receivers) and W (93.5 GHz, four receivers). All the data and products generated by WMAP can be found at the Legacy Archive for Microwave Background Data Analysis (LAMBDA) web site.¹

Following the WMAP team (Komatsu et al. 2003) we have performed our non-Gaussianity analyses on a noise weighted average of the Q, V and W receivers, which provides a CMB map where the signal-to-noise ratio has been increased. The K and Ka receivers are not included in the combined map since they are largely contaminated by Galactic foregrounds. In addition, the WMAP team has reduced the Galactic contamination present in the Q, V and W map by performing a foreground template fit as described in Hinshaw et al. (2007). In particular, the combined Q+V+W map is constructed using these clean data as (Bennett et al. 2003b):

$$T_c(\mathbf{x}) = \sum_{j=3}^{10} T_j(\mathbf{x}) w_j(\mathbf{x}), \quad (1)$$

¹ <http://cmbdata.gsfc.nasa.gov>

where \mathbf{x} gives the position in the sky and the index j correspond to the different receivers of the Q, V and W bands (i.e., the indices 3 to 10 refer to the Q1, Q2, V1, V2, W1, W2, W3 and W4 radiometers respectively). The noise weight $w_j(\mathbf{x})$ is defined as:

$$w_j(\mathbf{x}) = \frac{\bar{w}_j(\mathbf{x})}{\sum_{j=3}^{10} \bar{w}_j(\mathbf{x})}, \quad \bar{w}_j(\mathbf{x}) = \frac{N_j(\mathbf{x})}{\sigma_{0j}^2} \quad (2)$$

where σ_{0j} is the noise dispersion per observation for each radiometer given by Jarosik et al. 2007 and $N_j(\mathbf{x})$ is the number of observations made by the receiver j at the position in the sky \mathbf{x} .

Although the data are provided at a HEALPix² (Górski et al. 2005) resolution of $n_{side} = 512$, we degrade the data down to $n_{side} = 256$ since the smallest scales are dominated by noise. In addition, in order to avoid the strong contamination present at the Galactic plane and the emission coming from extragalactic point sources, only the data outside the WMAP Kp0 mask (Hinshaw et al. 2007), which corresponds approximately to 76 per cent of the sky, has been used. Finally, the monopole and dipole outside the Kp0 mask have been removed.

In order to apply our Gaussianity test, we construct the normalised temperature $u(\mathbf{x})$, which is obtained by dividing the data at each pixel by its corresponding expected dispersion. Since the contribution from residual foregrounds in the clean WMAP combined map outside the Kp0 is expected to be very small, the main contribution to the data dispersion comes from the CMB signal and the instrumental noise. The WMAP noise is very well approximated by Gaussian white noise at each pixel characterised by a dispersion $\sigma_n(\mathbf{x})$. Therefore, the normalised temperature is given by

$$u(\mathbf{x}) = \frac{T_c(\mathbf{x})}{\sqrt{\sigma_0^2 + \sigma_n^2(\mathbf{x})}} \quad (3)$$

where σ_0 is the CMB dispersion³ and has been estimated as

$$\sigma_0 = \sqrt{\sum_{\ell=2}^{\ell_{max}} \frac{2\ell+1}{4\pi} C_\ell^c} \quad (4)$$

The C_ℓ^c 's in the previous equation correspond to the power spectrum of the combined map assuming the best-fit model⁴ to the WMAP data and taking into account the different beams and noise weights used in the combination (see

² <http://healpix.jpl.nasa.gov>

³ Since the CMB is an homogeneous and isotropic field, σ_0 is constant over the sky. However, strictly speaking, there is a small dependence of σ_0 with the position in the WMAP combined map due to the different beams and noise weights used in the combination. Nonetheless, these differences are very small and one can assume, to a very good approximation, that the signal dispersion is constant over the sky.

⁴ The CMB simulations have been performed using the best-fit model – for the case of a Λ CDM model using only WMAP data – given in the first version of the papers of the three-year WMAP data release (Spergel et al. 2007, see table 5 of arXiv:astro-ph/0603449v1). Although the values of the cosmological parameters have been slightly modified in the final version of the WMAP papers, we have tested that these small changes do not affect the results of this work.

Table 1. The dispersion, skewness, kurtosis and Kolmogorov-Smirnov distance d_{KS} are given for the normalised WMAP data as well as for the northern and southern ecliptic hemispheres (in all cases considering only pixels outside the Kp0 mask). The significance of each quantity has been calculated from 1000 Gaussian realisations as the percentage of simulations with a value larger or equal to that obtained from the data.

Estimator	WMAP value	Signif. (%)
All pixels outside Kp0 mask		
dispersion	9.55×10^{-1}	97.8
skewness	-1.91×10^{-2}	74.7
kurtosis	1.49×10^{-2}	20.9
d_{KS}	1.21×10^{-2}	7.0
Northern ecliptic hemisphere		
dispersion	9.35×10^{-1}	99.4
skewness	2.17×10^{-2}	28.1
kurtosis	2.18×10^{-2}	20.1
d_{KS}	1.89×10^{-2}	25.2
Southern ecliptic hemisphere		
dispersion	9.76×10^{-1}	71.8
skewness	-5.85×10^{-2}	92.8
kurtosis	7.08×10^{-4}	35.4
d_{KS}	1.05×10^{-2}	67.3

Appendix A). The maximum ℓ that we have considered is $\ell_{max} = 2.5n_{side}$.

If the data follow a Gaussian distribution – and our assumptions about the underlying cosmological model and the instrumental noise are correct – the normalised temperature $u(\mathbf{x})$ should follow a Gaussian distribution with zero mean and unit dispersion $N(0,1)$.

We have calculated different estimators for the normalised data outside the Kp0 mask: dispersion, skewness and kurtosis. In addition, the data have been compared to a $N(0,1)$ distribution through a Kolmogorov-Smirnov test. In order to assign a significance to these quantities, the same analysis has been applied to 1000 Gaussian simulations of the WMAP combined data. To reproduce the data as closely as possible, the simulations have been generated at resolution $n_{side}=512$ for each radiometer and then processed in the same way as the data to obtain the simulated combined maps. Results are shown in Table 1. We find that the skewness and kurtosis are consistent with the results obtained from Gaussian simulations. However, the dispersion of the normalised data is significantly lower than expected, at the level of 97.8 per cent (i.e., only 22 out of the 1000 simulations have lower values than the one found for the data). Regarding the Kolmogorov-Smirnov distance (d_{KS}), we find that only 7 per cent of the simulations have a larger value of d_{KS} than the data. This could be related to the fact that the data dispersion is lower than expected, what would tend to produce a deviation of the normalised temperature from a $N(0,1)$ distribution. These deviations can also be seen in the top panel of Figure 1, which compares the histogram obtained from the normalised WMAP data with the one obtained averaging over 1000 Gaussian simulations. A deviation of the data histogram (dashed line) from the one

obtained with simulations (solid line) is apparent due to the small value of the dispersion of the normalised data. We would like to mention that the same analysis has also been performed on the first year WMAP data, finding again a low value of the dispersion (at a significance level of 99.5 per cent).

We may wonder if errors in the estimation of the WMAP noise level could affect the results of table 1. In particular, taking into account equation (3), an overestimation of the noise level would tend to bias the dispersion of the normalised temperature towards values lower than unity. Jarosik et al. (2007) use two different methods to estimate the noise level of each WMAP radiometer, finding that both methods agree within 0.3 per cent. This value can be considered as an indication of the level of error expected in the estimation of the WMAP noise. Even if we consider an overestimation of 1 per cent in the noise dispersion and recalculate, accordingly, the normalised temperature for the data, we still find a significant deviation for the dispersion. In particular, the new value of the dispersion is 0.956, which corresponds to a significance of 97.4 per cent. Therefore, the level of errors expected in the estimation of the noise level cannot explain this anomaly.

In order to investigate further the origin of this deviation, we have repeated the same analysis in the northern and southern ecliptic hemispheres, considering only those pixels outside the Kp0 mask (which correspond to a sky fraction of 38.8 and 37.0 per cent for the northern and southern hemispheres, respectively). Results are shown in Table 1. The values of skewness, kurtosis and d_{KS} remain compatible with Gaussian simulations. However, we find an asymmetry in the behaviour of the dispersion: while the data dispersion in the southern ecliptic hemisphere is compatible with the simulations (at the 71.8 per cent level), a clear deviation is found in the north, at the 99.4 per cent significance level (i.e., only 6 out of 1000 simulations had lower dispersion values). The middle (bottom) panel of Figure 1 shows the histogram of the data in the northern (southern) ecliptic hemisphere compared to the averaged histogram obtained from Gaussian simulations in the same sky region. The histogram obtained from the northern data shows again a systematic deviation from the average one, which is even larger than in the case of the whole sky, due to the lower value of the dispersion found for the data of the northern ecliptic hemisphere. Conversely, the histogram obtained from the southern data is closer to the average value of the Gaussian simulations.

3 STUDY OF THE CMB DISPERSION σ_0

Given the deviation found in the dispersion of the normalised temperature, we have performed a more detailed study of the CMB dispersion σ_0 . Let us recall that the dispersion of the data $\sigma(\mathbf{x})$ has contributions from both the CMB signal and the instrumental noise:

$$\sigma(\mathbf{x}) = \sqrt{\sigma_0^2 + \sigma_n^2(\mathbf{x})} \quad (5)$$

We have estimated the value of σ_0 by allowing this quantity to vary in equation (3) and compare the different obtained normalised temperatures to a Gaussian of zero mean and unit dispersion with the Kolmogorov-Smirnov test. Our estimation of the CMB dispersion is given by the value of σ_0

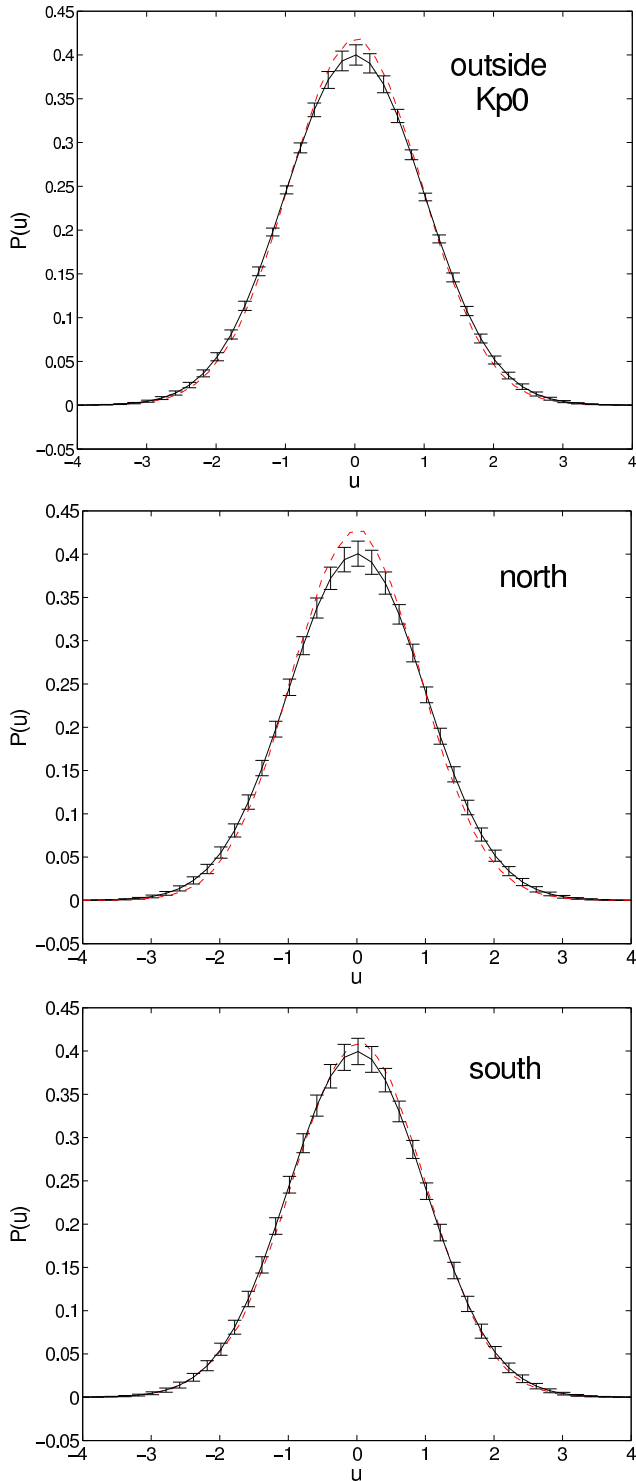


Figure 1. The top panel shows the histogram of the normalised WMAP data outside the Kp0 mask (dashed red line) compared to the averaged histogram obtained from 1000 simulations (solid black line). The error bars indicate the dispersion obtained from simulations. The middle and bottom panels give the same histograms for the northern and southern ecliptic hemispheres (only considering pixels outside the Kp0) respectively.

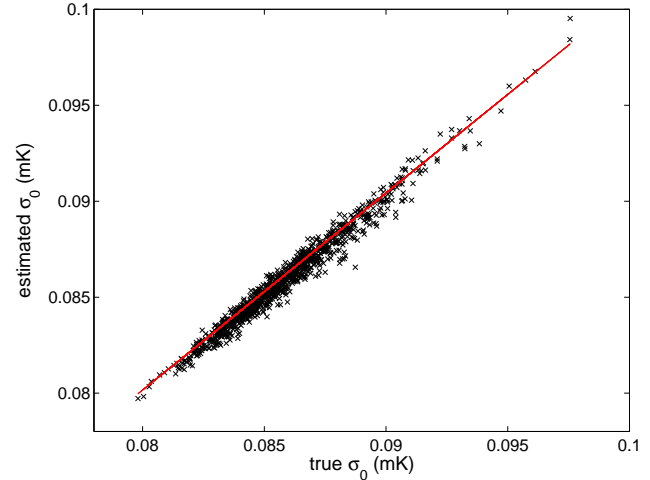


Figure 2. Estimated versus true dispersion (in mK) obtained from 1000 simulations of the WMAP combined map outside the Kp0 mask. For illustration, the best fit to a straight line is also shown (solid red line), which corresponds to $\hat{\sigma}_0 = 1.027\sigma_0 - 0.002$.

that produces the minimum d_{KS} . We have tested with simulations that this estimator performs well, as it will be shown below for the different considered cases.

Using this method, we have estimated a value of $\sigma_0 = 8.16 \times 10^{-2}$ mK for the WMAP combined map. The bias and error of this estimation has been tested using 1000 CMB simulations. Figure 2 shows the true CMB dispersion of each simulation outside the Kp0 mask versus the one estimated with our method from the simulated data in the same region of the sky. For illustration, the best fit to a straight line is also plotted, showing a very good correlation between the true and estimated dispersions. The bias (obtained as the average difference of the true minus the estimated dispersion) and error (obtained as the dispersion of the same difference) of the estimator are $b = -6.9 \times 10^{-5}$ mK and $e = 4.2 \times 10^{-4}$ mK respectively, i.e. the error of our estimator is at the level of ~ 0.5 per cent. In addition, the bias is also significantly smaller than the typical value expected for the CMB dispersion and therefore our estimator can be considered unbiased to a very good approximation. An additional bias in the estimated dispersion could also be present if the assumed level of instrumental noise were incorrect. In particular, an overestimation of the noise would imply an underestimation of the CMB dispersion. To check this possibility, we have also estimated σ_0 as $\langle T_1 T_2 \rangle$, with $T_1 = Q1 + V1 + W1 + W2$ and $T_2 = Q2 + V2 + W3 + W4$, finding a value which is consistent with the previous estimation within the 1σ error. Note that since instrumental noise is uncorrelated between channels, this latter estimation is not affected by a possible bias in the noise level.

For comparison, we have also calculated the mean σ_0 from 20000 noiseless CMB Gaussian simulations of the WMAP combined data, finding a value of 8.60×10^{-2} mK, clearly higher than the dispersion estimated for the data. In order to quantify the significance of this result, we have also obtained the distribution of variances from the same simulations. We find that 98.7 per cent of the simulations have a larger value of the variance (or, equivalently, of the

Table 2. The second column gives the CMB dispersion (in mK) estimated for the WMAP combined data obtained using pixels of three different regions of the sky: outside the Kp0, the northern ecliptic hemisphere outside the Kp0 and the southern ecliptic hemisphere outside the Kp0. In the third column, the mean dispersion value of the model, obtained averaging over 20000 Gaussian simulations, is given. Significances, that have been calculated as the percentage of simulations with values larger than the one found for the data using 20000 Gaussian CMB simulations, are given in the fourth column. Finally, in the last two columns, the bias (obtained as the average differences of the true minus the estimated dispersion) and error of the estimator, both in mK, are given, which have been obtained from 1000 Gaussian simulations.

Region	$\hat{\sigma}_0$	σ_0^{model}	Signif.	Bias	Error
Kp0	8.16×10^{-2}	8.60×10^{-2}	98.7	-6.9×10^{-5}	4.2×10^{-4}
north	7.97×10^{-2}	8.59×10^{-2}	99.8	-1.6×10^{-4}	6.8×10^{-4}
south	8.37×10^{-2}	8.59×10^{-2}	75.7	-2.0×10^{-4}	7.2×10^{-4}

dispersion) than the one found for the WMAP data. These results are summarised in Table 2.

It is interesting to point out that, for a Gaussian CMB, the distribution of the correlation function $C(\theta)$ for a given power spectrum can be analytically calculated (Cayón et al. 1991). In particular, we are interested in obtaining the theoretical distribution of the variance, i.e., the correlation function at $\theta = 0$. Following Cayón et al. (1991), the cumulative function of the variance can be calculated as

$$F(\sigma_0^2) = \frac{1}{2} + \frac{1}{\pi} \int_0^\infty \prod_{\ell=0}^{\ell_{max}} \left[(1 + 4t^2 \sigma_\ell^2)^{-\frac{2\ell+1}{4}} \right] \frac{\sin [B(t) + t\sigma_0^2]}{t} dt$$

$$B(t) = \sum_{\ell=0}^{\ell_{max}} \frac{2\ell+1}{2} \arctan(-2t\sigma_\ell), \quad (6)$$

where $\sigma_\ell = \frac{C_\ell}{4\pi}$ contains the power spectrum dependence. Calculating the derivative of the cumulative function with respect to σ_0^2 , we can also obtain the probability distribution of the variance:

$$p(\sigma_0^2) = \frac{1}{\pi} \int_0^\infty \prod_{\ell=0}^{\ell_{max}} \left[(1 + 4t^2 \sigma_\ell^2)^{-\frac{2\ell+1}{4}} \right] \cos [B(t) + t\sigma_0^2] dt \quad (7)$$

The previous distributions are valid when considering the variance of the whole sky. However, the presence of the Kp0 mask restricts the fraction of the sky (~ 76 per cent) used in the analysis. Since obtaining the significance of a given estimated CMB variance from simulations is significantly slower than calculating it from the cumulative function (6), we have tested whether the theoretical distributions are a good approximation in our case. The left panel of Figure 3 shows the cumulative function of σ_0^2 (black solid line) obtained using the theoretical power spectrum of the WMAP combined map calculated in Appendix A. The dotted-dashed blue line corresponds to the distribution of the variance obtained from 60000 Gaussian simulations over the whole sky. As expected, the agreement in this case is very good. Finally, the red dashed line gives the distribution of the variance obtained from the same simulations considering only those pixels outside the Kp0 mask. We can appreciate some small differences between this curve and the one obtained from equation (6), due to the fact that we are applying a mask, but the general agreement is very good. The maximum difference between both cumulative functions is found in the central part of the plot and is less than 0.04, whereas the differences in

the tails of the distributions are even smaller. Therefore, the theoretical cumulative function provides a simple and good approximation to obtain the significance of the estimated CMB variance in the considered case. In particular, using the theoretical distribution we obtain a significance of 99.3 per cent for the estimated σ_0 , that should be compared with the value of 98.7 obtained from simulations. Similar conclusions can be derived from the right panel of Figure 3, that shows the probability distribution of the variance for the same cases as before: theoretical (solid black line), from simulations using the whole sky (blue dotted-dashed line) and from simulations considering pixels outside Kp0 (red dashed-line).

Taking into account the results found in the previous section, we have also estimated the CMB dispersion in the northern and southern ecliptic hemispheres (considering only those pixels outside the Kp0 mask), obtaining values of 7.97×10^{-2} and 8.37×10^{-2} mK, respectively. The corresponding biases, errors, mean dispersion of the model and significances are given in Table 2. As expected, the bias and error of the estimator has increased slightly with respect to the ones obtained using all pixels outside the Kp0 mask, due to the smaller fraction of sky considered, but they are still small (less than 1 per cent with respect to $\hat{\sigma}_0$). In addition, it should be noted that this bias is negative, implying that, if anything, the CMB dispersion would tend to be overestimated and, therefore, the true σ_0 would be even lower.

We remark that the variance of the northern hemisphere is significantly low (only 0.2 per cent of the Gaussian simulations have lower values) whereas the southern hemisphere is compatible with the simulations. This is consistent with the results found in § 2, which seem to indicate that the anomaly found in the WMAP variance comes from the northern ecliptic hemisphere. This result is also in agreement with the lack of power found in the northern ecliptic hemisphere of the WMAP data by previous works (Eriksen et al. 2004; Hansen et al. 2004a; Eriksen et al. 2005).

We have also studied the ratio of σ_0^2 in the northern ecliptic hemisphere over σ_0^2 in the southern one for the WMAP data, finding that this quantity is consistent with what is expected from Gaussian simulations (with a significance of 88.7 per cent obtained from 20000 simulations). This can be explained because, although the value of σ_0 in the southern hemisphere is consistent with Gaussianity, this quantity is lower than the average dispersion expected from simulations, and this fact makes the north-south ratio compatible with the Gaussian model.

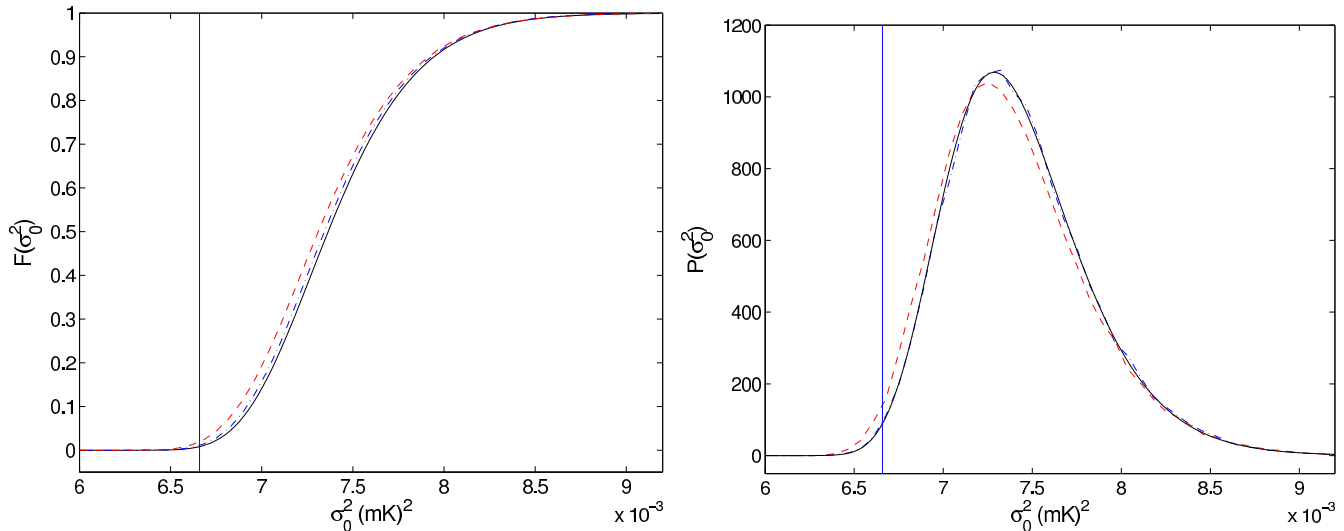


Figure 3. Left panel: theoretical cumulative function of the CMB variance (solid black line), compared to the same functions obtained from 60000 Gaussian simulations over the whole sky (blue dotted-dashed line) and using only the pixels outside the Kp0 mask (red dashed line). Right panel: the probability distribution of the variance is given for the three same cases. For illustration, the solid vertical line in both panels indicates the value obtained from the WMAP data. The units of the variance are $(mK)^2$.

Finally, we have studied the effect that the low CMB quadrupole measured by COBE (Bennett et al. 1996) and WMAP (Bennett et al. 2003a; Hinshaw et al. 2007) has in our results. Taking into account equation (4) and the fact that the C_ℓ 's are roughly proportional to $1/\ell(\ell+1)$, it is easy to see that the largest contributions to the CMB variance come from the lower multipoles and, in particular, from the quadrupole. In order to test if the low CMB quadrupole can be the origin of the low CMB variance we have repeated our analysis after removing the best-fit quadrupole (outside the Kp0 mask) from the data. With this procedure we find $\hat{\sigma}_0 = 8.07 \times 10^{-2}$ mK which corresponds to a theoretical significance of 96.9 per cent (obtained using equation (6) setting $C_2 = 0$). In addition, we have obtained the significance from 20000 simulations, where the quadrupole has been removed, finding a significance of 95.0 per cent. The same analysis has also been performed in the northern and southern ecliptic hemispheres, estimating for the dispersion 7.91×10^{-2} mK and 8.30×10^{-2} mK, respectively. The significances of these values, obtained from 20000 Gaussian simulations, are 99.2 and 44.3 per cent, respectively. Therefore, after removing the quadrupole, although the significances are slightly reduced, the CMB variance of the whole sky and that of the northern ecliptic hemisphere are still anomalously low. Thus, the low quadrupole cannot explain by itself these deviations.

4 DISCUSSION

We may wonder if the anomalous value found for the CMB dispersion in the WMAP data may have an extrinsic origin, i.e., to be due to the presence of some systematics or foreground residuals. In order to clarify this point, we have performed some further tests including an analysis of each individual radiometer (§4.1) as well as the study of the effect of $1/f$ noise (§4.2) and foreground residuals (§4.3).

4.1 Single radiometer analysis

In order to check if the low value of σ_0 found in the WMAP data could be explained by the presence of an anomalous radiometer, we have estimated the CMB dispersion from the maps of each radiometer following the method explained in §3. The results are summarised in Table 3. The mean dispersion σ_0^{model} and the significances (see §3) have been obtained analytically using the power spectrum of the WMAP best-fit model (Spergel et al. 2007) and taking into account the different beam window functions of each radiometer as well as the window pixel function of the considered resolution ($N_{side} = 256$). The biases and errors of the estimator have been obtained from 100 Gaussian simulations and are at a level less than 1 per cent in all cases.

As seen in Table 3, a different value of σ_0 has been obtained for each radiometer, which is expected due to the different beam window functions of each radiometer as well as to the statistical error of our estimator. In order to check if the dispersion of each radiometer is consistent with each other, and that no single radiometer has an anomalous dispersion that could be responsible for the low value of σ_0 found in the combined map, we have performed the following test. First, we have obtained the mean, d , and dispersion, $error(d)$, of the difference between the dispersion of the combined map minus that of each single radiometer from 100 simulations, where the map dispersions were obtained using our estimator. We have then added the corresponding mean difference d to the $\hat{\sigma}_0$ of each radiometer, which provides an estimation of σ_0 for the combined map (given in the sixth column of Table 3). If all the radiometer maps are consistent with each other, all these quantities should be compatible among them within the range allowed by the dispersion of the calculated differences (given in the seventh column of Table 3) as well as with the $\hat{\sigma}_0$ derived for the WMAP combined data. From Table 3, we see that consistency is found

Table 3. CMB dispersion (in mK) estimated from maps of individual radiometers outside the Kp0 mask. The mean dispersion of the model and the significances have been obtained analytically. The corresponding bias and error (in mK) have been obtained from 100 Gaussian simulations. For comparison, the same results obtained for the WMAP combined map are also shown. An estimation of the σ_0 of the combined map from each of the radiometers and its corresponding error are also given in the last two columns (see text for details).

Radiometer	$\hat{\sigma}_0$	σ_0^{model}	Signif. (%)	Bias	Error	$\hat{\sigma}_0 + d$	Error (d)
Q1	7.93×10^{-2}	8.34×10^{-2}	98.0	-4.9×10^{-5}	4.1×10^{-4}	8.21×10^{-2}	3.7×10^{-4}
Q2	7.88×10^{-2}	8.29×10^{-2}	97.9	4.1×10^{-6}	4.5×10^{-4}	8.21×10^{-2}	3.7×10^{-4}
V1	8.42×10^{-2}	8.84×10^{-2}	98.9	1.0×10^{-5}	4.4×10^{-4}	8.19×10^{-2}	3.7×10^{-4}
V2	8.46×10^{-2}	8.88×10^{-2}	98.8	-8.4×10^{-6}	3.7×10^{-4}	8.19×10^{-2}	3.6×10^{-4}
W1	8.66×10^{-2}	9.05×10^{-2}	98.3	-2.5×10^{-5}	5.4×10^{-4}	8.20×10^{-2}	5.7×10^{-4}
W2	8.48×10^{-2}	8.87×10^{-2}	98.1	-8.7×10^{-6}	5.8×10^{-4}	8.21×10^{-2}	6.6×10^{-4}
W3	8.47×10^{-2}	8.90×10^{-2}	99.1	1.1×10^{-4}	6.8×10^{-4}	8.16×10^{-2}	6.5×10^{-4}
W4	8.74×10^{-2}	9.07×10^{-2}	95.9	8.2×10^{-5}	5.8×10^{-4}	8.26×10^{-2}	5.9×10^{-4}
Combined	8.16×10^{-2}	8.62×10^{-2}	99.3	-6.9×10^{-5}	4.2×10^{-4}		

and that no single radiometer has an anomalous dispersion.⁵ Moreover, the significances obtained for the estimated dispersion for all the radiometers are significantly high, confirming that the anomaly cannot be attributed to a single radiometer.

In addition, we have repeated the same analysis for all the radiometers for each individual year of data. We find that the estimated CMB dispersion is reasonably stable along the three years of data for all the radiometers as well as for the combined map. This shows that the low σ_0 cannot be explained as the result of some anomaly in a single year of data.

4.2 1/f noise

In our analysis, it has been assumed that the WMAP instrumental noise is a Gaussian white noise characterised by a dispersion $\sigma_n(\mathbf{x})$ which varies with the position of the sky. Although this seems to be a very good approximation, the WMAP data also contain a small level of 1/f noise (Jarosik et al. 2003, 2007) and therefore we may wonder if this could be affecting our estimation of σ_0 .

In order to test the effect of 1/f noise we need realistic noise simulations that reproduce the WMAP data pipeline. As far as we know, this type of simulations are not available

for the three-year data but, however, the WMAP team did provide 110 of these simulations for each radiometer for the first year of data that include 1/f noise as well as all known radiometric effects (for details see the information in the LAMBDA web site).

Therefore, we have carried out the following test. First of all, we have combined the simulations of the different radiometers in the appropriate way in order to obtain 110 realistic noise simulations of the first-year WMAP combined map. We have then obtained the realistic noise dispersion map from these simulations. Since the number of simulations is relatively small, if we try to obtain the dispersion at each pixel, this map will be very noisy. Therefore, we have assumed that this quantity varies smoothly over the map and that neighbouring pixels would have the same level of noise. In particular, we have obtained the dispersion from 16 neighbouring pixels along the 110 simulations. The mean value of the ratio of this dispersion map over the one constructed assuming that only white noise is present is 1.02, which is an indication of the small level of 1/f noise present in the data.

The next step is to construct a new set of 110 realistic simulations by adding the combined realistic noise simulations to Gaussian CMB realizations of the WMAP combined first-year data. We have then applied our dispersion estimator to this new set of simulations and study its bias and error in 2 different cases: 1) including in equation (5) the value of $\sigma_n(\mathbf{x})$ obtained from the realistic noise simulations and 2) assuming that we have only white noise. Interestingly, the errors in both cases are very similar ($\sim 4 \times 10^{-4}$ mK), but the biases are significantly different. In the first case, when the noise is correctly characterised, the bias is very small (-3.4×10^{-5} mK), however, when only white noise is erroneously assumed, the bias increases to a value of -4.6×10^{-4} mK. This means that, if 1/f noise were present in the data and we did not properly take it into account, our estimation of the CMB dispersion would tend to shift towards higher values and, therefore, this effect could not explain an anomalous low value of σ_0 . This can be understood, since, by not including the 1/f noise, we are underestimating the level of instrumental noise and this extra power would tend to be compensated by increasing the signal dispersion. As a further test, we have estimated the CMB dispersion from the

⁵ Although consistency is found, it is observed that the dispersions derived from the radiometers are in general higher than that derived directly from the WMAP combined map. This small bias could be due to the presence of residual foregrounds and 1/f noise in the single radiometer maps, whose effect, as will be shown in sections §4.2 and §4.3, is to produce an overestimation of the dispersion in these maps. This is consistent with the fact that the radiometers that have a dispersion that deviates more from the one of the combined map (although always within the 2σ error) are Q1 and Q2, which are expected to be the channels more affected by residuals foregrounds, and W4, which presents the largest 1/f noise of all the radiometers (Jarosik et al. 2003). These possible residuals are expected to be reduced, relatively to the CMB signal, in the combined map and, therefore, the direct estimation of the σ_0 from the combined data would tend to give a lower (less biased) value than that obtained from each of the radiometers.

WMAP first-year data using the realistic noise dispersion map, finding a value of 8.12×10^{-2} mK to be compared with the larger dispersion obtained assuming white noise (8.17×10^{-2} mK).

Since there are not realistic noise simulations available for the WMAP three-year data, we cannot repeat this test for the complete set of data. However, we can qualitatively check that the same argument is valid for the three-year data using the reduced resolution inverse noise covariance matrices provided in the LAMBDA web site for the one and three-year data. The diagonal elements of the (direct) noise covariance matrices are dominated by white noise, whereas the off-diagonal elements come from $1/f$ noise. We have obtained the ratio of the diagonal and off-diagonal terms of the first-year data over the corresponding elements of the three-year data finding that, in both cases, this ratio peaks around 3. This means that the relative importance of the $1/f$ noise with respect to the white noise is approximately the same in both sets of data and, therefore, the effect that the $1/f$ noise has in the three-year data should be very similar to the one found for the first-year data.

Thus, residual $1/f$ noise cannot explain the low CMB variance found for the three-year WMAP data, since its unaccounted presence, if anything, would lead to higher values of $\hat{\sigma}_0$.

4.3 Foreground residuals

Although we are using the foreground cleaned maps provided by the WMAP team and applying a Galactic plus point source mask, some foreground residuals may still be present in the data. Therefore, it is interesting to test if this possible contamination can affect our estimation of the CMB dispersion.

An indication of a significant effect from foregrounds would be that the anomaly found in σ_0 was frequency dependent. However, from Table 3, we can see that this is not the case, since σ_0 is consistently low in the whole range of frequencies probed by Q, V and W (from 41 to 94 GHz).

In order to study further the effect of foreground contamination, we have estimated the value of σ_0 in the combined and individual radiometer maps without the foreground correction. The most relevant change is found for the Q1 and Q2 maps (lowering the significances of σ_0 down to 90.7 and 86.2 per cent respectively), whereas for the radiometers of the V and W bands, the changes are smaller. This is consistent with the fact that foreground emission is higher in the Q band and therefore the cleaning of the Q1 and Q2 maps is important to improve the estimation of the CMB dispersion. The presence of residuals also translates into a larger value for the $\hat{\sigma}_0$ of the combined map (8.23×10^{-2} mK).

As one would expect, these results indicate that if foreground residuals were present in the data, this would tend to bias σ_0 towards higher values. Therefore, the presence of foreground contamination cannot explain the anomaly found for the CMB dispersion.

Table 4. Ratio between the maximum value of the likelihood, when varying each parameter within a range given by 2 times the errors of the WMAP best fit model, over the likelihood of the best fit model (column 2) and significance of the variance for the model corresponding to this maximum likelihood value (column 3).

Parameters	Ratio	Signif.(%)
$\Omega_b h^2$	2.1	98.0
$\Omega_c h^2$	6.8	90.3
h	3.6	96.5
τ	10.1	68.5
n_s	11.9	79.0
A	14.1	57.5

5 POSSIBLE EXPLANATIONS OF THE ANOMALY

In all the analyses carried out in this work, we have assumed that the CMB fluctuations are isotropic and follow a Gaussian distribution characterised by a given power spectrum (which in turn is described by a particular cosmological model). However, since we have found an anomaly regarding the variance that cannot be easily explained by foregrounds or systematics, we may wonder if some of these assumptions are incorrect. In §5.1 we discuss if a different choice of cosmological parameters can make the estimated variance consistent with the model. In §5.2 we study if this anomaly can be due to a more fundamental reason: a deviation of the CMB from Gaussianity and/or isotropy.

5.1 Effect of cosmological parameters

During this work, we have used for the CMB power spectrum the best-fit model to the WMAP data assuming a flat Λ CDM model (Spergel et al. 2007). However, we would like to test if by varying the values of the cosmological parameters – within the current uncertainties – the estimated CMB variance could be more consistent with the theoretical expectations.

In order to test this possibility, we have considered the effect of varying the following cosmological parameters: the physical baryon density $\Omega_b h^2$, the physical cold dark matter density $\Omega_c h^2$, the reduced Hubble constant h , the reionization optical depth τ , the spectral index n_s and the amplitude of the density fluctuations A (with the constraint of having a flat Λ CDM model). Given that we have only one observable, the CMB variance σ_0^2 , modifying all the cosmological parameters simultaneously would lead to strong degeneracies between them. Therefore, as a first approach, we have studied the effect of varying one single parameter (within a range given by 2 times the errors of the WMAP best-fit model) while leaving the others unchanged. In particular, we have constructed the corresponding one-dimensional likelihoods in the following way: for each set of parameters, the CMB spectrum was calculated using CAMB (Lewis, Challinor & Lasenby 2000); this power spectrum was then inserted in equation (A8) in order to get the C_ℓ 's of the WMAP combined map; finally, the probability of having the observed value of σ_0^2 for that power spectrum was obtained using equation (7).

We find that the estimated CMB variance favours lower values of $\Omega_b h^2$, h and A than the ones of the best-fit model whereas higher values of $\Omega_c h^2$, n_s and τ are preferred. However, not all parameters are equally sensitive to the variance as can be seen in Table 4. This table gives the ratio between the maximum value of the likelihood, when varying one parameter in the considered range, over the likelihood of the WMAP best-fit model. The higher this ratio, the more sensitive the parameter to the CMB variance. We also show in Table 4 the significance of the variance for the model corresponding to this maximum likelihood value. We see that the compatibility of σ_0 with the model is only moderately improved when varying $\Omega_b h^2$, h and $\Omega_c h^2$ within the allowed range and the likelihood ratio also confirms that these parameters are not very sensitive to the value of the CMB variance. However, this ratio reaches higher values when considering the variation of A , τ and n_s and also the σ_0 becomes perfectly compatible with the model, showing that these three parameters are more relevant regarding this observable.

Taking into account the previous results, we have further investigated the effect of cosmological parameters by constructing the likelihood varying simultaneously the three more sensitive parameters, i.e. τ , n_s and A , while fixing the others to the values of the best-fit model. We find that there is a strong degeneracy between τ and A , and, therefore, we cannot extract any further information with the observed CMB variance regarding these two parameters. However, the situation is different for the spectral index. We have constructed the marginalized likelihood of n_s , finding that values of the spectral index higher than the ones given by the WMAP best-fit model are favoured. In particular, we find $\langle n_s \rangle = 0.98$, although one should point out that, as expected since we are using only one observable, the likelihood constructed in this way is significantly wider than the one obtained with the full power spectrum of the WMAP data.

Therefore it is possible to find models consistent with the estimated CMB variance by varying the value of the cosmological parameters in a certain range. However, in order for a model to be valid, it should still be compatible with the measured power spectrum. Thus, in principle, we should look for the model that best fits the data, allowing to vary all the cosmological parameters at the same time, subject to the constraint of compatibility with the estimated CMB variance. Unfortunately, in practice, this task is very complicated, and, as an illustration, we have just tried to find one model (not necessarily the best possible) that fits the WMAP power spectrum and is also consistent with the estimated CMB variance.

In order to find this model, we have carried out the following analysis. First we have selected a number (around 20) of sets of values of $\{\tau, n_s, A\}$ which are contained in the most probable 68 per cent of the 3-dimensional likelihood previously constructed for these parameters. For each of these sets, we have then run CosmoMC (Lewis & Bridle 2002) in order to find the best-fit to the WMAP data, with τ , n_s and A fixed for each set, varying the rest of the cosmological parameters. From all the considered models, we find that the one that best fits the WMAP power spectrum has the values given in Table 5. It is interesting to note that the value of the spectral index is higher ($n_s = 0.983$) for the new model. As seen in Figure 4 the model fits reasonably well the

Table 5. Estimated cosmological parameters for the WMAP best-fit and for an illustrative model more consistent with the estimated variance.

Parameters	Best-fit	New model
$100\Omega_b h^2$	$2.23^{+0.07}_{-0.09}$	2.27
$\Omega_c h^2$	$0.104^{+0.007}_{-0.010}$	0.089
h	$0.73^{+0.03}_{-0.04}$	0.81
τ	$0.088^{+0.028}_{-0.034}$	0.132
n_s	$0.951^{+0.015}_{-0.019}$	0.983
A	$0.80^{+0.04}_{-0.05}$	0.75

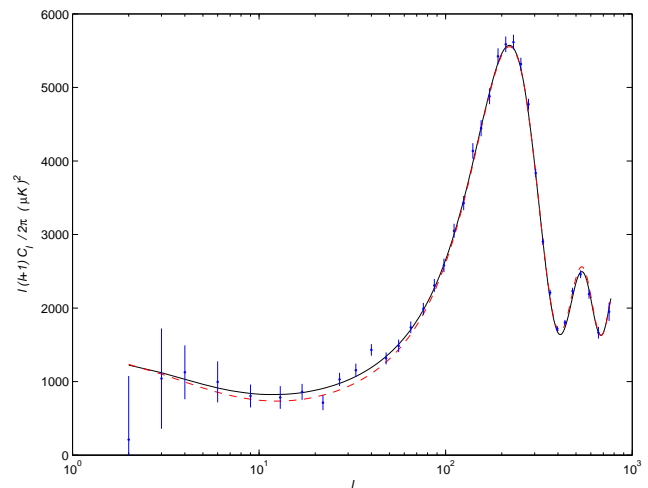


Figure 4. The power spectrum for the WMAP best-fit model (solid black line) and for an illustrative model more consistent with the estimated variance (red dashed line) are shown. For comparison, the binned power spectrum measured from the WMAP three-year data (blue points) is also plotted (Spergel et al. 2007).

power spectrum and the main difference can be found at low l 's where the new model (red dashed line) goes below the WMAP best-fit (black solid line), which would tend to give a smaller variance. In particular, we find that the estimated variance has a theoretical significance of 93.1 per cent for this new model (to be compared with 99.3 found for the WMAP best-fit) and therefore the CMB variance is not so significantly low in this case.

Therefore, this seems to indicate that the low value of the CMB dispersion found in the WMAP data could be made compatible with the model, while keeping a reasonable fit to the power spectrum, by varying the cosmological parameters. In addition, we would like to point out again that we have considered only a restricted set of models and if the whole set of cosmological parameters were allowed to vary simultaneously, it is likely that we would find models that would fit better both the estimated variance and the power spectrum. Nonetheless, a more exhaustive study where a wider range of models were considered would be necessary to confirm this result.

5.2 Gaussianity and isotropy of the CMB

A deviation of the CMB from Gaussianity and/or isotropy could also explain the inconsistency found between the estimated CMB variance and the considered model. Moreover, this possibility is also supported by the fact that different authors have claimed the presence of departures from Gaussianity and/or isotropy in the WMAP data (see §1).

One possible way to test the Gaussianity and isotropy of the CMB is to perform a consistency test of the data using equation (4), that relates the CMB variance and the power spectrum. Gaussianity and isotropy have been assumed to estimate both, the CMB variance and the WMAP power spectrum. Therefore, if these assumptions are valid, both results should be consistent.

To perform this test, we have used the actual measured power spectrum of the WMAP data⁶, i.e. the power spectrum estimated for the particular realization of the CMB sky, instead of the best-fit model. From these C_ℓ 's, we have calculated the power spectrum that we expect for the WMAP combined map (using the results of Appendix A). Finally, we have calculated the value of the CMB variance from equation (4) using this power spectrum of the combined map. In this way, we find a value for the dispersion of 8.40×10^{-2} mK. The error associated to this quantity is expected to be small, since the main contribution to the variance is due to the low multipoles, which are almost unaffected by the instrumental noise. This value should be compared to $(8.16 \pm 0.04) \times 10^{-2}$ mK, the dispersion that we have previously estimated from the combined map. The difference between these two estimations indicates the presence of an inconsistency in the data between the measured power spectrum and the estimated variance.

To study further this possibility we have also calculated the theoretical significance of our estimated CMB variance from equation (6), using again the power spectrum of the WMAP combined map constructed from the actual measured WMAP power spectrum (instead of the best-fit model as done in §3). In this case, we find a value of 96.0 per cent for the significance. Moreover, if we remove the quadrupole from the data (as explained in §3), the significance increases to 99.5 per cent⁷. This points out again towards an inconsistency between the estimated values of the variance and those of the power spectrum in the WMAP data (independently of the best-fit model). In addition, it also shows that the anomaly is present at multipoles higher than the quadrupole.

Therefore, a deviation from Gaussianity and/or isotropy of the WMAP data could be the reason for the inconsistency found between the estimated variance and the

considered model. Moreover, taking into account the results of §4, that show that the anomalously low variance cannot be explained by known systematics or foregrounds (and assuming that the estimated CMB power spectrum is neither affected by spurious signals), a cosmological origin for this deviation from Gaussianity and/or isotropy cannot be discarded.

6 CONCLUSIONS

We have studied the normalised temperature distribution of the CMB using the WMAP data, finding that the skewness, kurtosis and the Kolmogorov-Smirnov test are consistent with Gaussianity. However, the dispersion was significantly lower (at the level of 97.8 per cent) than expected from CMB simulations using the WMAP best-fit power spectrum. This result was even more significant when only the northern ecliptic sky was considered (at 99.4 per cent). In order to clarify this point, a more detailed analysis of the CMB dispersion of the WMAP data has been performed. In particular, we have estimated this dispersion to be 8.16×10^{-2} mK, which is again anomalously low (98.7 per cent of the Gaussian CMB simulations have a larger value of the dispersion). If only the northern ecliptic hemisphere is considered, the significance increases to 99.8 per cent, whereas the southern ecliptic hemisphere is compatible with the simulations.

We have repeated our analysis using single radiometer and single year maps, finding that the significance of the low variance is practically frequency independent and that it cannot be explained by an anomalous radiometer or by an artifact in a single year data. In addition, the presence of residual foregrounds or $1/f$ noise cannot explain the low value of the CMB dispersion, since they would tend to shift $\hat{\sigma}_0$ towards higher values.

We have also investigated the effect of varying the cosmological parameters in the significance of the estimated variance. In particular, searching within a restricted number of models, we have found one case that provides a reasonable fit to the WMAP power spectrum and for which the significance of the estimated variance decreases to 93.0 per cent. This seems to indicate that is possible to find a model that is consistent with both the estimated variance and the measured power spectrum of the WMAP data, especially if a wider range of cosmological models is considered. Nevertheless, a more exhaustive study is necessary to confirm this result. It is also interesting to point out that the CMB variance tends to favour higher values of the spectral index than the full-power spectrum analysis of the WMAP data.

Finally, we have considered the possibility that a deviation from Gaussianity and/or isotropy could be the reason for the anomalous variance. We find that there is an inconsistency between the estimated CMB variance and the actual measured power spectrum of the WMAP data, independently of the best-fit model. This indicates that a deviation from Gaussianity and/or isotropy could be a possible explanation for the found anomaly. Moreover, taking into account that known systematics or foregrounds cannot explain the anomalously low CMB variance, a cosmological origin for this possible deviation cannot be discarded.

⁶ The power spectrum measured for the three-year WMAP data is available at the LAMBDA web site.

⁷ In §3, when removing the quadrupole, the significance of the variance decreased (unlike in the current analysis). This makes sense, since the quadrupole of the data is known to be significantly lower than that of the best-fit model, and therefore removing the quadrupole from the analysis would make the variance more consistent with the best-fit model. However, in the current analysis, we are comparing the estimated CMB variance with the actual measured power spectrum of the WMAP data, where the quadrupole is also low and, therefore, removing the quadrupole, does not necessarily increase the consistency.

ACKNOWLEDGMENTS

The authors thank P. Mukherjee for help regarding cosmological parameter estimation, M. Cruz, A. Curto, D. Heranz, M. López-Cañiego, and J.L. Sanz for useful discussions and R. Marco for the computational support. CM thanks the Spanish Ministerio de Ciencia y Tecnología (MCyT) for a predoctoral FPI fellowship and for two grants to visit The Cavendish Laboratory of the University of Cambridge (UK). CM, RBB, PV and EMG thank the Cavendish Laboratory for their hospitality during several research stays and also acknowledge partial financial support from the Spanish projects ESP2004-07067-C03-01 and AYA2007-68058-C03-02. Some of the results in this paper have been derived using the HEALPix (Górski et al., 2005) package. We acknowledge the use of the Legacy Archive for Microwave Background Data Analysis (LAMBDA). Support for LAMBDA is provided by the NASA Office of Space Science. We acknowledge the use of the software CAMB (<http://camb.info/>) developed by A. Lewis and A. Challinor and of CosmoMC developed by A. Lewis and S. Bridle.

REFERENCES

- Aghanim N., Forni O., Bouchet F.R., 2001, *A&A*, 365, 341
 Aliaga A.M., Rubiño-Martín J.A., Martínez-González E., Barreiro R.B., Sanz J.L., 2005, *MNRAS*, 356, 1559
 Barreiro R.B., Sanz J.L., Martínez-González E., Silk J., 1998, *MNRAS*, 296, 693
 Barreiro R.B., Hobson M.P., Lasenby A.N., Banday A.J., Górski K.M., Hinshaw G., 2000, *MNRAS*, 318, 475
 Barreiro R.B., Martínez-González E., Sanz J.L., 2001, *MNRAS*, 322, 411
 Barreiro R.B., Hobson M.P., 2001, *MNRAS*, 327, 813
 Bartolo N., Komatsu E., Matarrese S., Riotto A., 2004, *Phys. Rep.*, 402, 103
 Bennett, C.L. et al, 1996, *ApJS*, 464, L1
 Bennett, C.L. et al, 2003a, *ApJS*, 148, 1
 Bennett, C.L. et al, 2003b, *ApJS*, 148, 97
 Bernui A., Villela T., Wuensche C.A., Leonardi R., Ferreira, 2006, *A&A*, 454, 409
 Bernui A., Mota B., Reboucas M.J., Tavakol R., 2007, *A&A*, 464, 479
 Cayón L., Martínez-González E., Sanz J.L., 1991, *MNRAS*, 253, 599
 Cayón L., Jin J., Treaster A., 2005, *MNRAS*, 362, 826
 Chiang L., Naselsky P.D., Verkhodanov O.V., 2003, *ApJ*, 590, L65
 Chiang L.-Y., Naselsky P., Coles P., 2004, *ApJ*, 602, L1
 Coles P., 1988, *MNRAS*, 234, 509
 Coles P., Barrow J.D., 1987, *MNRAS*, 228, 407
 Coles P., Dineen P., Earl J., Wright D., 2004, *MNRAS*, 350, 989
 Copi C.J., Huterer D., Starkman G.D., 2004, *Phys. Rev. D.*, 70, 043515
 Copi C.J., Huterer D., Schwarz D.J., Starkman G.D., 2007, *Phys. Rev. D.*, 75, 023507
 Cruz M., Martínez-González E., Vielva P., Cayón L., 2005, *MNRAS*, 356, 29
 Cruz M., Tucci M., Martínez-González E., Vielva P., 2006, *MNRAS*, 369, 57
 Cruz M., Cayón L., Martínez-González E., Vielva P., Jin J., 2007, *ApJ*, 655, 11
 Curto A., Aumont J., Macías-Pérez J.M., Martínez-González E., Barreiro R.B., Santos D., Désert F.X., Tristram M., 2007, *A&A*, 474, 23
 de Oliveira-Costa A., Tegmark M., Zaldarriaga M., Hamilton A., 2004, *Phys. Rev. D*, 69, 063516
 Doré O., Colombi S., Bouchet F.R., 2003, *MNRAS*, 344, 905
 Durrer R., 1999, *New Astron. Rev.*, 43, 111
 Eriksen H.K., Hansen F.K., Banday A.J., Górski K.M., Lilje P.B., 2004, *ApJ*, 605, 14
 Eriksen H.K., Banday A.J., Górski K.M. and Lilje P.B., 2005, *ApJ*, 622, 58
 Eriksen H.K., Banday A.J., Górski K.M., Hansen F.K., Lilje P.B., 2007, *ApJ*, 660, L81
 Ferreira P.G., Magueijo J., Górski K.M., 1998, *ApJ*, 503, L1
 Górski K.M., Hivon E., Banday A.J., Wandelt B.D., Hansen F.K., Reinecke M., Bartelmann M., 2005, *ApJ*, 622, 759
 Gott III J.R., Park C., Juszkievicz R., Bies W.E., Bennett D.P., Bouchet F.R., Stebbins A., 1990, *ApJ*, 352, 1
 Hajian A., Souradeep T., 2003, *ApJ*, 597, L5
 Hansen F.K., Banday A.J., Górski K.M., 2004a, *MNRAS*, 354, 641
 Hansen F.K., Cabella P., Marinucci D., Vittorio N., 2004b, *ApJ*, 607, L67
 Heavens A.F., 1998, *MNRAS*, 299, 805
 Heavens A.F., Sheth R.K., 1999, *MNRAS*, 310, 1062
 Hinshaw G. et al., 2007, *ApJS*, 170, 288
 Hivon E., Górski K.M., Netterfield C.B., Crill B.P., Prunet S., Hansen F., 2002, *ApJ*, 567, 2
 Hobson M.P., Jones A.W., Lasenby A.N., 1999, *MNRAS*, 309, 125
 Jarosik N., 2003, *ApJS*, 148, 29
 Jarosik N. et al., 2007, *ApJS*, 170, 263
 Komatsu E. et al., 2003, *ApJS*, 148, 119
 Land K., Magueijo J., 2005a, *Phys. Rev. Lett.*, 95, 071301
 Land K., Magueijo J., 2005b, *MNRAS*, 357, 994
 Larson D.L., Wandelt B.D., 2004, *ApJ*, 613, L85
 Lewis A., Challinor A., Lasenby A., 2000, *ApJ*, 538, 473
 Lewis A., Bridle S., 2002, *Phys. Rev. D*, 66, 103511
 Magueijo J., 2000, *ApJ*, 528, L57
 Martínez-González E., Barreiro R.B., Diego J.M., Sanz J.L., Cayón L., Silk J., Mollerach S., Martínez V.J., 2000, *ApL&C*, 37, 335
 Martínez-González E., Cruz M., Cayón L., Vielva P., 2006, *New Astronomy Review*, 50, 875
 McEwen J.D., Hobson M.P., Lasenby A.N., Mortlock D.J., 2005, *MNRAS*, 359, 1583
 McEwen J.D., Hobson M.P., Lasenby A.N., Mortlock D.J., 2006, *MNRAS*, 371, L50
 Monteserín C., Barreiro R.B., Sanz J.L., Martínez-González E., 2005, *MNRAS*, 360, 9
 Monteserín C., Barreiro R.B., Martínez-González E., Sanz J.L., 2006, *MNRAS*, 371, 312
 Mukherjee P., Wang Y., 2004, *ApJ*, 613, 51
 Naselsky P., Novikov D., 1995, *ApJ*, 444, L1
 Rubiño-Martín, J.A. et al., 2006, *MNRAS*, 369, 909
 Schwarz D.J., Starkman G.D., Huterer D., Copi C.J., 2004, *Phys. Rev. Lett.*, 93, 221301

- Spergel D.N. et al., 2007, ApJS, 170, 377
 Vielva P., Martínez-González E., Barreiro R.B., Sanz J.L., Cayón L., 2004, ApJ, 609, 22
 Vielva P., Wiaux Y., Martínez-González E., Vandergheynst P., 2007, MNRAS, 381, 932
 Wiaux Y., Vielva P., Martínez-González E., Vandergheynst P., 2006, Phys. Rev. Lett., 96, 151303
 Wiaux Y., Vielva P., Barreiro R.B., Martínez-González E., Vandergheynst P., 2008, MNRAS, in press (astro-ph/0706.2346)

APPENDIX A: THEORETICAL POWER SPECTRUM OF A COMBINED MAP

The derivation of the angular power spectrum of the CMB signal present in the combined Q-V-W map C_ℓ^c is given in this appendix. This combined map, $T_c(\vec{x})$, is the linear combination (see equation 1) of the eight cleaned maps ($T_i(\vec{x})$ with i running from 3 to 10) at different WMAP frequencies (Q1 and Q2 at 41 GHz, V1 and V2 at 61 GHz, and W1, W2, W3 and W4 at 94 GHz). Let us recall here the explicit formula:

$$T_c(\vec{x}) = \sum_{i=3}^{10} w_i(\vec{x}) T_i(\vec{x}), \quad (\text{A1})$$

where $T_i(\vec{x})$ is the CMB observation made by the i radiometer and the coefficients $w_i(\vec{x})$ represent, at a given position \vec{x} , the relative weight given to the noise dispersion for each radiometer, and are normalized to unity (see equation 2).

Each CMB observation made by the i radiometer can be expressed in terms of the spherical harmonic coefficients of the pure CMB signal $a_{\ell m}$, the beam (b_ℓ^i) and pixel (p_ℓ) window functions:

$$T_i(\vec{x}) = \sum_{\ell, m} a_{\ell m} b_\ell^i p_\ell Y_{\ell m}(\vec{x}) \quad (\text{A2})$$

Let us define $\tilde{T}_i(\vec{x}) = w_i(\vec{x}) T_i(\vec{x})$ as the noise-weighted CMB signal observed by the radiometer i . It is straightforward to show that the angular power spectrum of the combined CMB signal is given by:

$$C_\ell^c = \sum_{i,j} \tilde{C}_\ell^{ij} = \sum_{i,j} \frac{1}{2\ell+1} \sum_m \tilde{a}_{\ell m}^i \tilde{a}_{\ell m}^{j*} \quad (\text{A3})$$

where \tilde{C}_ℓ^{ij} is the cross-angular power spectrum of the CMB signal between the i and the j radiometers and $\tilde{a}_{\ell m}^i$ are the spherical harmonic coefficients of the noise-weighted CMB signal observed by the radiometer i :

$$\begin{aligned} \tilde{a}_{\ell m}^i &= \int d\Omega \tilde{T}_i(\vec{x}) Y_{\ell m}^*(\vec{x}) = \int d\Omega w_i(\vec{x}) T_i(\vec{x}) Y_{\ell m}^*(\vec{x}) = \\ &= \sum_{\ell' m'} a_{\ell' m'} b_{\ell'}^i p_{\ell'} \int d\Omega w_i(\vec{x}) Y_{\ell m}^*(\vec{x}) Y_{\ell' m'}(\vec{x}) = \\ &= \sum_{\ell' m'} a_{\ell' m'} b_{\ell'}^i p_{\ell'} K_{\ell m \ell' m'}^i. \end{aligned} \quad (\text{A4})$$

$K_{\ell m \ell' m'}^i$ is a matrix introducing coupling among multipoles due to the noise-weighting.

Including equation (A4) in equation (A3), the the angular power spectrum of the combined CMB signal reads:

$$\begin{aligned} C_\ell^c &= \sum_{i,j} \frac{1}{2\ell+1} \sum_m \tilde{a}_{\ell m}^i \tilde{a}_{\ell m}^{j*} \\ &= \sum_{i,j} \frac{1}{2\ell+1} \sum_m \left(\sum_{\ell', m'} a_{\ell' m'} b_{\ell'}^i p_{\ell'} K_{\ell m \ell' m'}^i \right) \times \\ &\quad \left(\sum_{\ell'', m''} a_{\ell'' m''} b_{\ell''}^j p_{\ell''} K_{\ell m \ell'' m''}^j \right)^* = \\ &= \sum_{i,j} \frac{1}{2\ell+1} \sum_{\ell'} C_{\ell'} b_{\ell'}^i b_{\ell'}^j p_{\ell'}^2 \times \\ &\quad \sum_{m, m'} K_{\ell m \ell' m'}^i K_{\ell m \ell' m'}^{j*}. \end{aligned} \quad (\text{A5})$$

where $C_{\ell'}$ is the angular power spectrum of the pure CMB signal and we have applied $\sum_{\ell', m'} \sum_{\ell'', m''} a_{\ell', m'} a_{\ell'', m''}^* = \sum_{\ell', m'} C_{\ell'} \delta_{\ell' \ell''} \delta_{m' m''}$.

The coupling $K_{\ell m \ell' m'}^i$ can be expressed in terms of the Wigner $3j$ -symbols and the spherical harmonic coefficients ($w_{\ell m}$) of the noise-weights, as follows:

$$\begin{aligned} K_{\ell m \ell' m'}^i &= \int d\Omega w_i(\vec{x}) Y_{\ell m}^*(\vec{x}) Y_{\ell' m'}(\vec{x}) = \\ &= \sum_{\ell'', m''} w_{\ell'' m''}^i \int d\Omega Y_{\ell m}^*(\vec{x}) Y_{\ell' m'}(\vec{x}) Y_{\ell'' m''}(\vec{x}) = \\ &= \sum_{\ell'', m''} \left\{ w_{\ell'' m''}^i (-1)^{m'} \left[\frac{(2\ell+1)(2\ell'+1)(2\ell''+1)}{4\pi} \right]^{\frac{1}{2}} \right. \\ &\quad \left. \begin{pmatrix} \ell & \ell' & \ell'' \\ 0 & 0 & 0 \end{pmatrix} \begin{pmatrix} \ell & \ell' & \ell'' \\ m & -m' & m'' \end{pmatrix} \right\} \end{aligned} \quad (\text{A6})$$

One of the orthogonality properties of the Wigner-3j symbols reads (see e.g. Hivon et al. 2002):

$$\sum_{m_1, m_2} \begin{pmatrix} \ell_1 & \ell_2 & \ell_3 \\ m_1 & -m_2 & m_3 \end{pmatrix} \begin{pmatrix} \ell_1 & \ell_2 & \ell_4 \\ m_1 & -m_2 & m_4 \end{pmatrix} = \frac{1}{2\ell_3+1} \delta_{\ell_3 \ell_4} \delta_{m_3 m_4} \delta(\ell_1, \ell_2, \ell_3) \quad (\text{A7})$$

where $\delta(\ell_1, \ell_2, \ell_3) = 1$ when the triangular relation $|\ell_1 - \ell_2| \leq \ell_3 \leq \ell_1 + \ell_2$ is satisfied.

Replacing equation (A6) in equation (A5) and taking into account equation (A7), it is straightforward to derive the final expression for the angular power spectrum of the combined CMB signal:

$$\begin{aligned} C_\ell^c &= \sum_{i,j} \sum_{\ell'} C_{\ell'} b_{\ell'}^i b_{\ell'}^j p_{\ell'}^2 \frac{2\ell'+1}{4\pi} \times \\ &\quad \sum_{\ell''} (2\ell''+1) w_{\ell''}^{ij} \begin{pmatrix} \ell & \ell' & \ell'' \\ 0 & 0 & 0 \end{pmatrix}^2, \end{aligned} \quad (\text{A8})$$

where $w_{\ell''}^{ij}$ is the cross-angular power spectrum of the noise-weights between the radiometers i and j .

In order to test the performance of this approach, the theoretical angular power spectrum of the combined Q-V-W WMAP three-year map (at $n_{side}=256$ resolution) given

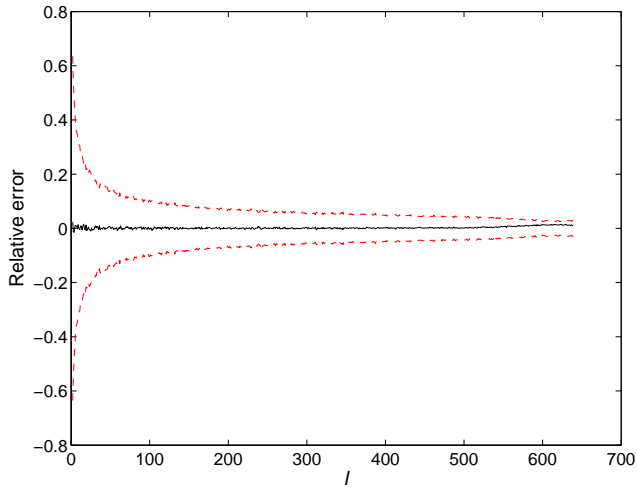


Figure A1. Relative error (solid black line) of the theoretical angular power spectrum of the WMAP combined map, given by equation (A8), with respect to the one averaged from 1000 simulations. The relative error is obtained as the difference of the theoretical C_ℓ 's minus the average ones, and this difference is divided by the average C_ℓ 's. The dashed red lines give the 1σ errors (obtained from the simulations) divided by the averaged angular power spectrum from simulations.

by the above equation has been compared with the angular power spectrum obtained from the average of 1000 Gaussian simulations of the combined map. In Figure A1, the relative error between both spectra is given (solid black line) up to $\ell = 2.5n_{side}$. The red dashed lines give the relative 1σ error (obtained from the simulations). The agreement between both angular power spectra in the considered range is very good.